Manuscript prepared for Earth Syst. Sci. Data
with version 2015/09/17 7.94 Copernicus papers of the LaTeX class copernicus.cls.
Date: 20 October 2017

Using CALIOP to estimate cloud-field base height and its uncertainty

Johannes Mülmenstädt[1], Odran Sourdeval[1], Tristan S. L'Ecuyer[2], Christoph Böhm[3], and Johannes Quaas[1]

[1]Institute of Meteorology, Universität Leipzig, Leipzig, Germany
[2]University of Wisconsin, Madison, USA
[3]Institute for Geophysics and Meteorology, Universität zu Köln, Köln, Germany

Correspondence to: Johannes Mülmenstädt (johannes.muelmenstaedt@uni-leipzig.de)

Abstract. A technique is presented that uses attenuated backscatter profiles from the CALIOP satellite lidar to estimate cloud base heights. Even when clouds are thick enough to attenuate the lidar beam (optical thickness $\tau \gtrsim 5$), the technique provides cloud base heights by treating the cloud base height of nearby thinner clouds as representative of the surrounding cloud field. Using ground-based ceilometer data, uncertainty estimates for the cloud base height product at retrieval resolution are derived as a function of various properties of the CALIOP lidar profiles. Evaluation of the predicted cloud base heights and their predicted uncertainty using a second, statistically independent, ceilometer dataset shows that cloud base heights and uncertainties are biased by less than 10%. Geographic distributions of cloud base height and its uncertainty are presented. Regionally, the uncertainty is found to be substantially smaller than the 480 m uncertainty assumed in the A-Train downwelling longwave estimate, potentially permitting the most uncertain of the radiative fluxes in the climate system to be better constrained.

1 Introduction

Cloud base height (CBH) is an important geometric parameter of a cloud. It controls how much downwelling longwave radiation the cloud emits. Aerosol concentration and updraft speed at that level determine the microphysical characteristics of the cloud. It is one of the parameters that is required in the calculation of the subadiabaticity of the cloud. However, due to the viewing geometry, it is also one of the most difficult cloud parameters to retrieve from satellite.

Multiple methods have been proposed for satellite determination of the cloud base height. Zhu et al. (2014) have used the Visible Infrared Imaging Radiometer Suite aboard the Suomi National Polar-orbiting Partnership satellite (VIIRS, Cao et al., 2014) to estimate cloud base temperature (CBT) from the lowest cloud-top temperature within a cloud cluster; a reanalysis temperature profile can be used to convert CBT to CBH. Using an empirical relationship between geometric and optical thickness, Fitch et al. (2016) have obtained CBH from VIIRS. Cloud geometric thickness (and

therefore CBH if the cloud top height is known) can be inferred from increased spectral absorption by O_2 within cloud due to multiple scattering (Kokhanovsky and Rozanov, 2005). Stereoscopic determination of the height of the most reflective layer (Naud et al., 2005, 2007) in Multiangle Imaging Spectroradiometer data (MISR, Diner et al., 1998) yields information on CBH, as the lowest layer heights within a cloud cluster may correspond to the base of a cloud seen from its side. An evaluation of MISR techniques is in progress (Böhm et al., 2017).

For analyses wishing to combine cloud base information with other cloud properties retrieved by A-Train satellites, these methods share the disadvantage that the required instruments are not part of the A-Train. Methods that are applicable to A-Train satellites are based on Moderate Resolution Imaging Spectroradiometer (MODIS, Platnick et al., 2017) cloud properties retrieved near cloud top and integrated along moist adiabats to determine the cloud thickness (Meerkoetter and Zinner, 2007) or on active remote sensing by CloudSat (2B-GEOPROF, Marchand et al., 2008) or a combination of CloudSat and CALIOP (2B-GEOPROF-LIDAR, Mace and Zhang, 2014). Each of these has drawbacks. The MODIS-derived cloud thickness assumes adiabatic cloud profiles and therefore cannot be used to constrain subadiabaticity; the use of ancillary temperature profile estimates may also be problematic in many cases. CloudSat misses the small droplets at the base of nonprecipitating clouds, and retrievals are further degraded in the ground clutter region. CALIOP detects the bases of only the thinnest clouds ($\tau < 5$, Mace and Zhang, 2014); frequently, it is desirable to know the base height of thick clouds as well.

In this paper, we revisit the CALIOP cloud base determination. This relies on one central assumption, namely that, because the lifting condensation level is approximately homogeneous within an airmass, the cloud bases retrieved by CALIOP for thin clouds may be a good proxy for the cloud base heights of an entire cloud field, including the optically thicker clouds within the field. We have designed an algorithm that extrapolates the CALIOP cloud-base measurements into locations where CALIOP attenuates before reaching cloud base. This algorithm is called CBASE (Cloud Base Altitude Spatial Extrapolator). In this paper we evaluate its performance by comparing CBASE CBH against CBH observed by ground-based ceilometers.

The cloud base of interest in this analysis is the base of the lowest cloud in each column. Even if it CALIOP can also detect the base heights of other layers in multilayer situations, it is the base height of the lowest cloud that is of largest interest for many applications (e.g., surface radiation estimates).

Section 2 describes the data sources used in determining and evaluating CBH. In Section 3 we describe the algorithm and evaluate its performance, including error statistics. The publicly available processed CBASE output is described in Section 4. We conclude in Section 5 with an outlook on the longstanding questions that the CBASE dataset can address.

2 Data

Two classes of data are used in this work: cloud lidar data, from which we intend to derive a global CBH dataset; and ground-based observations used as reference measurements of CBH to train and evaluate the algorithm by which CBH is determined from the satellite data.

2.1 CALIOP VFM

The input satellite data to our analysis is from the Cloud-Aerosol Lidar with Orthogoncal Polarization (CALIOP Winker et al., 2007) on board the Cloud-Aerosol Lidar and Infrared Pathfinder Satellite Observation (CALIPSO) satellite that is part of the A-Train satellite constellation (Stephens et al., 2002) on a sun-synchronous low-Earth orbit with equator crossings at approximately 1330 hours local time. The cloud-base product relies on the retrieved vertical feature mask (VFM, vau). For each CALIOP lidar backscatter profile, the VFM identifies features such as clear air, cloud, aerosol, or planetary surface; this is termed the "feature type". (When the lidar beam is completely attenuated, this is reported as a feature type.) In addition to the feature type, the VFM records the degree of confidence in the identification ("none" to "high", termed the "feature type QA flag"); the thermodynamic phase of a layer identified as cloud as well as the degree of confidence therein (termed "ice water phase" and "ice water phase QA flag"); the horizontal distance over which the algorithm had to average to identify a feature above noise and molecular atmospheric scattering ("horizontal averaging distance").

In the present analysis, we use VFM version 4.10 (CALIPSO Science Team, 2016), the current "standard" release, for the years 2007 and 2008. The VFM files are obtained from ICARE (ica).

2.2 Airport ceilometers

For optimizing several parameters of the algorithm, for determining the expected cloud base uncertainty, and for evaluation of the trained algorithm, reference measurements of CBH are required. The source of these "true" CBH in this work is ground-based cloud observations at airports. Weather observations at airports are disseminated worldwide in aviation routine and special weather reports (METARs and SPECIs, collectively referred to as METARs henceforth, World Meteorological Organization, 2013). Apart from providing airport weather information for aviation, METAR data is used for assimilation into numerical weather prediction (NWP) models (e.g., Benjamin et al., 2016; Dee et al., 2011). In many locations, CBH reported in METARs is measured by a ceilometer over a period of time (tens of minutes) and then objectively grouped into cloud layers and their respective fractional coverages, using the temporal variation at a fixed point under an advected cloud field as a proxy for spatial variability of the cloud field (e.g., Heese et al., 2010). METAR data is widely distributed and archived; the data for the present analysis was downloaded from the Weather Underground archive (wun).

In the United States, CBH is mostly derived automatically by laser ceilometers that form part of Automated Surface Observing Stations (ASOS, National Oceanic and Atmospheric Administration, Department of Defense, Federal Aviation Administration, and United States Navy, 1998) system; see, e.g., An et al. (2017); Ikeda et al. (2017) for recent examples of ASOS application to deriving cloud climatologies or NWP model evaluation. In other parts of the world, the cloud bases may be estimated by human observers or may be omitted under certain conditions when the lowest cloud base is higher than 5000 feet, complicating objective comparison to satellite CBH. To ensure that the ceilometer CBH are of high and spatially uniform quality, we restrict ourselves to METARs from the contiguous continental United States.

There are 1645 stations throughout the continental USA that lie within 100 km of a CALIOP footprint. In normal operation, the time resolution of CBH reports is 1 h, but during rapidly changing conditions, more frequent updates may be provided; for comparison to satellite CBH, the ceilometer observation closest in time to the satellite overpass is used, provided that the time difference is less than 1 h. For training the algorithm, we use ceilometer observations from the year 2008. For unbiased evaluation of the algorithm performance, a statistically independent dataset is required; we use ceilometer observations from the same stations from the year 2007. Figure 1 shows the locations of these stations along with the number of satellite–ceilometer CBH coincidences and the closest co-location distance during the year 2007.

3 CBASE Algorithm and evaluation

The CBASE algorithm and evaluation proceed in four steps:

1. We determine the CBH from all CALIOP profiles where the surface generates a return, indicating that the lidar is not completely attenuated by cloud. We refer to this as the *local CBH* in the sense that it is local to the CALIOP profile.

2. Using ground-based ceilometer data, we determine quality of cloud base height depending on a number of properties of the CALIOP profile. Assuming those properties suffice to determine the quality of the CBH estimate, we can then predict the quality of a cloud base as a function of those factors. The quality metric we use is the root mean square error (RMSE); the category RMSE determined from comparison to ceilometer CBH then serves as the predicted CBH uncertainty. In the language of machine learning, we refer to this step as *training* the algorithm on the ceilometer data to predict CBH and CBH uncertainty.

3. Based on the predicted quality of each local cloud base, we either reject the local cloud base or combine it with other local cloud bases within a distance $D_{\max}$ of the point of interest (POI) to arrive at an estimate of the CBH and its uncertainty at the POI.

4. Using a statistically independent validation dataset, we verify that the predicted CBH and its uncertainty are correct.

This section is divided into four subsections, one for each algorithm step enumerated above.

3.1 Determination of local CBH

Local CBH is determined from the CALIOP VFM for each profile with a surface return. The rationale is that a surface return indicates that the lidar did not attenuate within the cloud, and that the lower limit of the layer identified as cloud therefore corresponds to the cloud base; Figure 2 illustrates the idea. For these profiles, the location, CBH, cloud top height, feature type between the cloud base and the surface, cloud thermodynamic phase, and associated quality assurance flags from the VFM algorithm are recorded.

3.2 Determination of local cloud base quality

We assess the quality of the CALIOP CBH z using the root mean square error (RMSE) with respect to the ceilometer-observed CBH $\hat{z}$. The RMSE is defined as

$$E = \sqrt{\frac{1}{N}\sum_{i=1}^{N}(z_i - \hat{z})^2}. \tag{1}$$

The sum runs over all CALIOP profiles containing at least one cloud layer and a surface return that are within 100 km horizontal distance of the ceilometer, occurred within 3600 s of a ceilometer observation, and have their lowest CALIOP cloud feature within 3 km of the surface. Ceilometer observations are only used if the observation closest in time to the Calipso overpass contains a cloud within 3 km of the surface. This height limit is imposed because a subset of the ceilometers has a range limit of 12500 feet, and all ceilometers report ceilings above 10000 feet with reduced granularity (500 feet); the 3 km threshold is safely below these ceilometer limitations and mimics the International Satellite Cloud Climatology Project (ISCCP, Rossow and Schiffer, 1999) definition of low cloud ($p > 680$ hPa).

The following metrics, which are useful for a qualitative assessment of the quality of the satellite cloud base, are also calculated, but play no quantitative role in the algorithm:

Correlation coefficient between the CALIOP cloud base and ground-based observation of the cloud base. We use the Pearson correlation coefficient (ideally unity).

Linear regression slope and intercept (ideally 1 and 0, respectively).

Retrieval bias, defined as

$$\text{bias} = \frac{1}{N}\sum_{i=1}^{N}(z_i - \hat{z}), \tag{2}$$

(ideally 0)

Efficiency, i.e., probability that a retrieval is available at the desired location (ideally 1).

CALIOP's ability to detect cloud base depends on the properties of the cloud. Therefore, we expect that the CBH quality will vary between different cloud profiles. Measuring the quality as a function of various properties of the CALIOP column may allow us to predict the quality of other columns with the same combination of properties. The properties that are easily accessible in a single column and have substantial effects on quality are:

- horizontal distance D from the ceilometer,
- number of column cloud bases within horizontal distance $D_{\max}$,
- CALIOP VFM feature quality assurance flag,
- geometric thickness of the lowest cloud layer,
- CALIOP thermodynamic phase determination of lowest cloud,
- feature type, if any, detected between the lowest cloud and the surface,
- and horizontal averaging distance required for CALIOP cloud feature detection.

For illustrative purposes, Figure 3 shows the joint distribution of CALIOP and ceilometer CBH faceted by the CALIOP VFM feature quality assurance flag.

Based on determining the retrieval quality as a function of one variable at a time (integrating over the sample distribution of the remaining variables), the following classes of CALIOP profiles are discarded:

- CALIOP VFM quality assurance worse than "high" ,
- "invalid" or "no signal" layers between the surface and the lowest cloud layer (indicating that although the surface may generate a detectable return, the lidar is sufficiently attenuated that the cloud base, which scatters less strongly than the surface, is unreliable),
- minimum CALIOP cloud detection horizontal averaging distance within the lowest cloud layer greater than 1 km (indicating that, although average cloud properties are known at the averaging length scale, those properties may not be representative of the particular CALIOP footprint under consideration), or
- thermodynamic phase of the lowest layer determined to be other than liquid by the CALIOP VFM algorithm (the reason for this is that not enough such columns exist to determine the RMSE reliably in each of the categories defined below).

The remaining variables are discretized roughly into quintiles of their distribution within the VFM dataset with the following boundaries:

– horizontal distance D from the ceilometer, with boundaries 0, 40, 60, 75, 88, and 100 km (distance greater than 100 km is discarded),

– number of CALIOP columns n with a cloud layer and a surface return within 100 km horizontal distance from the ceilometer, with boundaries at 0, 175, 250, 325, 400 (multiplicities greater than 400 are accepted),

– geometric thickness Δz of the lowest cloud layer, with boundaries at 0, 0.25, 0.45, 0.625, and 1 km (thickness greater than 1 km is accepted).

We can now consider the joint distribution of CALIOP and ceilometer cloud bases for each combination of the above variables to derive the RMSE of each combination. For this comparison, we use CBH above ground level (AGL); using CBH above mean sea level (MSL) would introduce an intrinsic correlation between satellite and ceilometer CBH due to the varying terrain height, which would lead to an unrealistically positive assessment.

When calculating aggregate statistics such as the RMSE, a further consideration comes into play. CBH above ground is positive-definite, which imposes a physical phase-space boundary. Due to this boundary, the satellite CBH estimate is intrinsically biased high (negative excursions may be removed by the phase-space boundary, but positive excursions are not), and the bias decreases with increasing satellite CBH estimate (when true CBH is high, it is less likely that measurement error would lead to a negative AGL CBH). Since this effect constitutes a bias rather than a random error, it cannot be eliminated by averaging over large sample sizes, but instead needs to be corrected for. Since the effect is nonlinear in CBH, a nonlinear correction method is required; our choice of nonlinear bias correction is an ε-regression support vector machine (SVM, Chang and Lin, 2011).

Following bias correction, the sample RMSE is calculated for each combination of D, n, and Δz. The sample RMSE is taken as an estimate of the statistical uncertainty $\sigma(D,n,\Delta z)$ on the CALIOP CBH.

3.3 Combination of local cloud bases

CALIOP CBH only exists sporadically, when CALIOP happens to hit a sufficiently thin cloud. To infer the CBH z at a point of interest (POI) that does not necessarily coincide with the location of a thin-cloud CALIOP profile, we proceed as follows. We first select all local CALIOP CBH measurements within a horizontal distance $D_{\max} = 100$ km of the POI that satisfy the additional quality cuts described in Section 3.2.

For each remaining local CBH z_i, we determine the predicted uncertainty σ_i based on the categories established in the previous section. We determine a combined CBH

$$z = \frac{\sum_i^n w_i z_i}{\sum_i^n w_i} \tag{3}$$

with weights

$$w_i = \frac{1}{\sigma_i^2} \tag{4}$$

(optimal weights for uncorrelated least-squares). In practice, the individual measurements of cloud base are highly correlated with fairly similar σ_i. The cloud base estimate by Eq. (3) with weights given by Eq. (4) remains unbiased even in the presence of correlations. However, for the combined cloud base uncertainty, the uncorrelated weights would yield a biased estimate in the presence of correlations. The expression

$$\sigma^2 = \frac{1}{n}\sum_i^n \sigma_i^2 \tag{5}$$

yields acceptable results, as would be expected for highly correlated and fairly similar σ_i.

3.4 Evaluation of CBASE CBH and CBH errors

Having trained the algorithm on data from the year 2008, we evaluate it using a statistically independent dataset from the year 2007. In the evaluation dataset, the "true" (i.e., ceilometer-measured) CBH $\hat{z}$ is known in addition to the estimated CBH z and the estimated CBH uncertainty σ, determined according to the procedure described in the previous section. Figure 4 shows the joint distribution of CBASE and ceilometer-observed CBH. (The difference between this figure and Figure S3 is that the underlying data is the validation (2007), rather than the training (2008), dataset.)

For satellite-derived measurements of the CBH z that are unbiased with respect to the ceilometer-observed CBH $\hat{z}$ and have correctly estimated uncertainties σ, the pdf of the quantity $(z-\hat{z})/\sigma$ has zero mean and unit standard deviation. In our evaluation dataset, we find a mean of 0.04 and a standard deviation of 1.06, shown in Figure 5; this corresponds to a CBH bias of 4% and uncertainty bias of 6%, both relative to the predicted uncertainty. Thus, we find that both the cloud base estimate and the uncertainty estimate are unbiased at better than the 10% level.

As a further test of the reliability of the expected uncertainty, we divide the validation dataset into deciles of the expected uncertainty. Table 2 shows that the actual RMSE within each decile is within 10% of the expected uncertainty (with the exception of the highest-uncertainty decile) and that linear regressions within each decile are close to the one-to-one line.

It is possible that CBH estimates outside North America could have greater biases or greater uncertainty than this evaluation leads us to believe. This would be the case if continental clouds over North America are not representative of clouds elsewhere in a way that is not accounted for by the cloud properties considered by the uncertainty estimate. Since the validation sample spans an entire year on a continental scale, we expect that most cloud morphologies are included. However, cloud types that occur predominantly over ocean present a particular challenge to the method, namely marine stratocumulus with horizontally extensive but vertically thin liquid-phase anvils. Due to the typical CBH uncertainty of several hundred m, the method is unlikely to be applied to stratocumulus cloud;

nevertheless, a marine-cloud validation dataset would be desirable. For the present work, no suitable marine-cloud evaluation dataset was available; ship-based CBH observations were either based on human observers with coarse vertical resolution and a precision that is difficult to characterize; or available only over a limited duration at limited locations, resulting in a severely statistics-limited set of coincidences with the CALIOP track.

4 Results and data product availability

Geographic distributions of the mean CBH are shown for daytime and nighttime Calipso overpasses in Figure 6. Over most of the globe, especially over land, daytime CBH is higher than nighttime CBH, consistent with the diurnal deepening of the planetary boundary layer. Figures 7 and 8 show the distribution of CBH uncertainties. A larger fraction of nighttime cloud bases falls into the lowest uncertainty range (200 to 350 m), while the the nighttime uncertainty distribution peaks somewhat higher than the daytime uncertainty distribution. CALIOP benefits from higher signal to noise ratio during nighttime, which may lead to lower CBH uncertainty, but this effect would be convoluted with potential differences between daytime and nighttime clouds that can lead to different CBH uncertainties.

Comparison with 2B-GEOPROF-LIDAR cloud bases is shown in Figure 9. 2B-GEOPROF-LIDAR distinguishes between radar-only, lidar-only, and radar–lidar combined cloud bases; the latter category is rare for warm cloud and is not shown. For radar-only clouds, the mean error is large because the radar CBH predominantly clusters around the top of the ground clutter region with little dependence on the actual CBH. Lidar-only 2B-GEOPROF-LIDAR cloud base performs comparably to the CBASE cloud base on average; this is to be expected, as the underlying physical measurement is the same. Unlike 2B-GEOPROF-LIDAR, CBASE provides a validated uncertainty estimate, which allows an analysis to select only low-uncertainty cases or to statistically weight CBH according to uncertainty, as appropriate for the application.

As an example application, (Stephens et al., 2012a, b) use an assumed 2B-GEOPROF-LIDAR CBH uncertainty of 480 m. By selecting the lowest-uncertainty percentile of the cloud population, the CBH uncertainty can be reduced to approximately 250 m at night in the extratropics and in the SCu regions, and approximately 400 m throughout the tropics during daytime, according to Figure 8. This reduces the available statistics by a factor of 100, but the A-Train is not statistics-limited.

The CBASE CBH and CBH uncertainty dataset (Mülmenstädt et al., 2017) is freely available at Deutsches Klimarechenzentrum (DKRZ) under doi:10.123/456789. {j_μ: Add DOI once it is available.}

5 Conclusions

We have presented the CBASE algorithm, which derives CBH from CALIOP lidar profiles. This algorithm produces CBH not only for thin clouds but also for clouds thick enough to attenuate the lidar (optical thickness $\tau \gtrsim 5$), based on the assumed mesoscale homogeneity of cloud base height within an airmass. In addition to the CBH estimate, the CBASE algorithm supplies an expected uncertainty on the CBH. The CBASE data is available for the years 2007 and 2008 at {j_μ: insert DOI}.

CBASE CBH and its uncertainty have been evaluated using ground-based airport ceilometer data over the contiguous United States, using a data sample unbiased by the training of the algorithm. The evaluation showed that CBH and CBH uncertainty are unbiased at the better than 10% level: the bias on the CBH is 4%, and the bias on the uncertainty is 6%, both relative to the expected uncertainty.

The performance of CBASE CBH is similar to that of 2B-GEOPROF-LIDAR lidar-only CBH, which are based on the same underlying physical measurement. However, the validated CBH uncertainty provided by CBASE allows for selection of only accurate cloud base heights or for statistically weighting of CBH according to expected uncertainty. This, in turn, makes the CBASE CBH useful for pressing problems in climate research that require accurate knowledge of cloud geometry, such as cloud subadiabaticity, which will be presented in future work.

Acknowledgements. We thank ICARE for hosting the CALIOP VFM dataset, which was originally obtained from the NASA Langley Research Center Atmospheric Science Data Center. We thank the Deutsches Klimarechenzentrum (DKRZ) for computing and data hosting. This research was funded by the European Union under grant agreement 306284 ERC Starting grant QUAERERE.

References

http://www.icare.univ-lille1.fr/catalogue/, {j_μ: still trying to figure out how to cite these websites}.

https://www-calipso.larc.nasa.gov/resources/pdfs/PC-SCI-202_Part2_rev1x01.pdf.

http://www.wunderground.com/history/airport/.

An, N., Wang, K., Zhou, C., and Pinker, R. T.: Observed Variability of Cloud Frequency and Cloud-Base Height within 3600m above the Surface over the Contiguous United States, JOURNAL OF CLIMATE, 30, 3725–3742, doi:10.1175/JCLI-D-16-0559.1, 2017.

Benjamin, S. G., Weygandt, S. S., Brown, J. M., Hu, M., Alexander, C. R., Smirnova, T. G., Olson, J. B., James, E. P., Dowell, D. C., Grell, G. A., Lin, H., Peckham, S. E., Smith, T. L., Moninger, W. R., Kenyon, J. S., and Manikin, G. S.: A North American Hourly Assimilation and Model Forecast Cycle: The Rapid Refresh, MONTHLY WEATHER REVIEW, 144, 1669–1694, doi:10.1175/MWR-D-15-0242.1, 2016.

Böhm, C., Sourdeval, O., Mülmenstädt, J., and Quaas, J.: Heavenly fluff: clouds in stereo, in preparation, 2017.

CALIPSO Science Team: CALIPSO/CALIOP Level 2, Vertical Feature Mask Data, version 4.10, doi:10.5067/CALIOP/CALIPSO/LID_L2_VFM-Standard-V4-10, {j_μ: ironically, ESSD has no author recommendation on data DOI citation format; this is the `@misc` format}, 2016.

Cao, C., De Luccia, F. J., Xiong, X., Wolfe, R., and Weng, F.: Early On-Orbit Performance of the Visible Infrared Imaging Radiometer Suite Onboard the Suomi National Polar-Orbiting Partnership (S-NPP) Satellite, IEEE TRANSACTIONS ON GEOSCIENCE AND REMOTE SENSING, 52, 1142–1156, doi:10.1109/TGRS.2013.2247768, 2014.

Chang, C.-C. and Lin, C.-J.: LIBSVM: A library for support vector machines, ACM Transactions on Intelligent Systems and Technology, 2, 27:1–27:27, software available at http://www.csie.ntu.edu.tw/~cjlin/libsvm, 2011.

Dee, D. P., Uppala, S. M., Simmons, A. J., Berrisford, P., Poli, P., Kobayashi, S., Andrae, U., Balmaseda, M. A., Balsamo, G., Bauer, P., Bechtold, P., Beljaars, A. C. M., van de Berg, L., Bidlot, J., Bormann, N., Delsol, C., Dragani, R., Fuentes, M., Geer, A. J., Haimberger, L., Healy, S. B., Hersbach, H., Holm, E. V., Isaksen, L., Kallberg, P., Koehler, M., Matricardi, M., McNally, A. P., Monge-Sanz, B. M., Morcrette, J.-J., Park, B.-K., Peubey, C., de Rosnay, P., Tavolato, C., Thepaut, J.-N., and Vitart, F.: The ERA-Interim reanalysis: configuration and performance of the data assimilation system, QUARTERLY JOURNAL OF THE ROYAL METEOROLOGICAL SOCIETY, 137, 553–597, doi:10.1002/qj.828, 2011.

Diner, D. J., Beckert, J. C., Reilly, T. H., Bruegge, C. J., Conel, J. E., Kahn, R. A., Martonchik, J. V., Ackerman, T. P., Davies, R., Gerstl, S. A. W., Gordon, H. R., Muller, J. P., Myneni, R. B., Sellers, P. J., Pinty, B., and Verstraete, M. M.: Multi-angle Imaging SpectroRadiometer (MISR) - Instrument description and experiment overview, IEEE TRANSACTIONS ON GEOSCIENCE AND REMOTE SENSING, 36, 1072–1087, doi:10.1109/36.700992, 1998.

Fitch, K. E., Hutchison, K. D., Bartlett, K. S., Wacker, R. S., and Gross, K. C.: Assessing VIIRS cloud base height products with data collected at the Department of Energy Atmospheric Radiation Measurement sites, INTERNATIONAL JOURNAL OF REMOTE SENSING, 37, 2604–2620, doi:10.1080/01431161.2016.1182665, 2016.

Heese, B., Flentje, H., Althausen, D., Ansmann, A., and Frey, S.: Ceilometer lidar comparison: backscatter coefficient retrieval and signal-to-noise ratio determination, ATMOSPHERIC MEASUREMENT TECHNIQUES, 3, 1763–1770, doi:10.5194/amt-3-1763-2010, 2010.

Ikeda, K., Steiner, M., and Thompson, G.: Examination of Mixed-Phase Precipitation Forecasts from the High-Resolution Rapid Refresh Model Using Surface Observations and Sounding Data, WEATHER AND FORECASTING, 32, 949–967, doi:10.1175/WAF-D-16-0171.1, 2017.

Kokhanovsky, A. A. and Rozanov, V. V.: Cloud bottom altitude determination from a satellite, IEEE GEOSCIENCE AND REMOTE SENSING LETTERS, 2, 280–283, doi:10.1109/LGRS.2005.846837, 2005.

Mace, G. G. and Zhang, Q.: The CloudSat radar-lidar geometrical profile product (RL-GeoProf): Updates, improvements, and selected results, JOURNAL OF GEOPHYSICAL RESEARCH-ATMOSPHERES, 119, 9441–9462, doi:10.1002/2013JD021374, 2014.

Marchand, R., Mace, G. G., Ackerman, T., and Stephens, G.: Hydrometeor detection using Cloudsat - An earth-orbiting 94-GHz cloud radar, JOURNAL OF ATMOSPHERIC AND OCEANIC TECHNOLOGY, 25, 519–533, doi:10.1175/2007JTECHA1006.1, 2008.

Meerkoetter, R. and Zinner, T.: Satellite remote sensing of cloud base height for convective cloud fields: A case study, GEOPHYSICAL RESEARCH LETTERS, 34, L17 805, doi:10.1029/2007GL030347, 2007.

Merk, D., Deneke, H., Pospichal, B., and Seifert, P.: Investigation of the adiabatic assumption for estimating cloud micro- and macrophysical properties from satellite and ground observations, ATMOSPHERIC CHEMISTRY AND PHYSICS, 16, 933–952, doi:10.5194/acp-16-933-2016, 2016.

Mülmenstädt, J., Sourdeval, O., L'Ecuyer, T., Böhm, C., and Quaas, J.: CBASE cloud base height estimate, version 1.0, doi:10.123/456789, 2017.

National Oceanic and Atmospheric Administration, Department of Defense, Federal Aviation Administration, and United States Navy: Automated Surface Observing System User's Guide, http://www.nws.noaa.gov/asos/pdfs/aum-toc.pdf, 1998.

Naud, C. M., Muller, J. P., Clothiaux, E. E., Baum, B. A., and Menzel, W. P.: Intercomparison of multiple years of MODIS, MISR and radar cloud-top heights, ANNALES GEOPHYSICAE, 23, 2415–2424, 2005.

Naud, C. M., Baum, B. A., Pavolonis, M., Heidinger, A., Frey, R., and Zhang, H.: Comparison of MISR and MODIS cloud-top heights in the presence of cloud overlap, REMOTE SENSING OF ENVIRONMENT, 107, 200–210, doi:10.1016/j.rse.2006.09.030, 2007.

Platnick, S., Meyer, K. G., King, M. D., Wind, G., Amarasinghe, N., Marchant, B., Arnold, G. T., Zhang, Z., Hubanks, P. A., Holz, R. E., Yang, P., Ridgway, W. L., and Riedi, J.: The MODIS Cloud Optical and Microphysical Products: Collection 6 Updates and Examples From Terra and Aqua, IEEE TRANSACTIONS ON GEOSCIENCE AND REMOTE SENSING, 55, 502–525, doi:10.1109/TGRS.2016.2610522, 2017.

Rossow, W. B. and Schiffer, R. A.: Advances in understanding clouds from ISCCP, BULLETIN OF THE AMERICAN METEOROLOGICAL SOCIETY, 80, 2261–2287, doi:10.1175/1520-0477(1999)080<2261:AIUCFI>2.0.CO;2, 1999.

Stephens, G. L., Vane, D. G., Boain, R. J., Mace, G. G., Sassen, K., Wang, Z. E., Illingworth, A. J., O'Connor, E. J., Rossow, W. B., Durden, S. L., Miller, S. D., Austin, R. T., Benedetti, A., and Mitrescu, C.: The cloudsat mission and the a-train - A new dimension of space-based observations of clouds and precipitation,

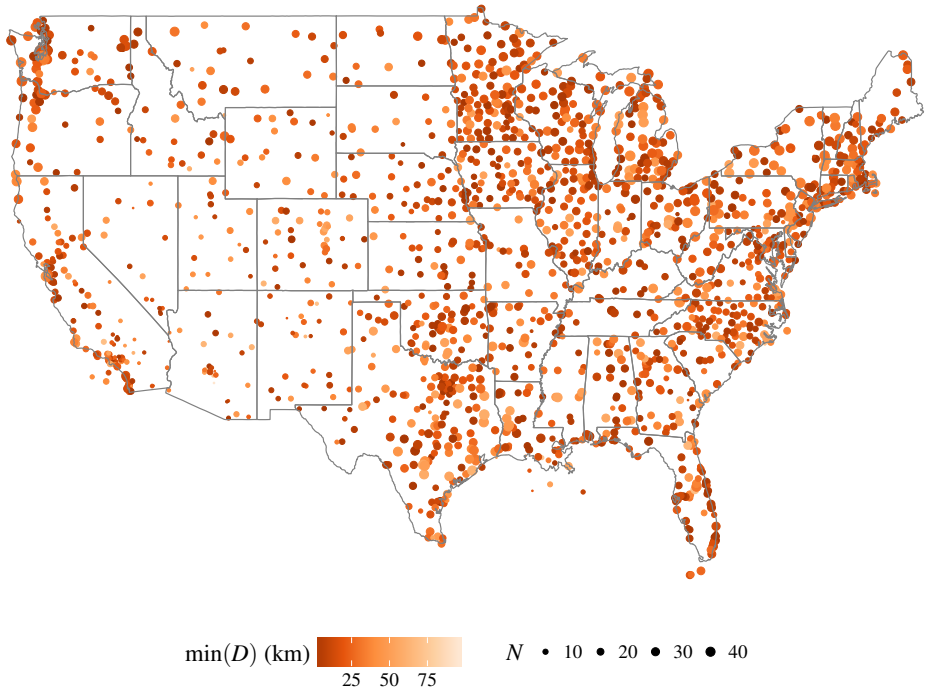

Figure 1. ASOS ceilometers used for CBASE CBH evaluation. The size of the marker indicates the number of satellite–ceilometer CBH coincidences during the year 2007. Color indicates the closest co-location distance achieved in 2007.

BULLETIN OF THE AMERICAN METEOROLOGICAL SOCIETY, 83, 1771–1790, doi:10.1175/BAMS-83-12-1771, 2002.

Stephens, G. L., Li, J., Wild, M., Clayson, C. A., Loeb, N., Kato, S., L'Ecuyer, T., Stackhouse, P. W. J., Lebsock, M., and Andrews, T.: An update on Earth's energy balance in light of the latest global observations, NATURE GEOSCIENCE, 5, 691–696, doi:10.1038/NGEO1580, 2012a.

Stephens, G. L., Wild, M., Stackhouse, P. W. J., L'Ecuyer, T., Kato, S., and Henderson, D. S.: The Global Character of the Flux of Downward Longwave Radiation, JOURNAL OF CLIMATE, 25, 2329–2340, doi:10.1175/JCLI-D-11-00262.1, 2012b.

Winker, D. M., Hunt, W. H., and McGill, M. J.: Initial performance assessment of CALIOP, GEOPHYSICAL RESEARCH LETTERS, 34, L19 803, doi:10.1029/2007GL030135, 2007.

Wood, S. N.: Fast stable restricted maximum likelihood and marginal likelihood estimation of semiparametric generalized linear models, Journal of the Royal Statistical Society (B), 73, 3–36, 2011.

World Meteorological Organization: Techincal Regulations Volume II: Meteorological service for international air navigation, https://library.wmo.int/pmb_ged/wmo_49-v2_2013_en.pdf, 2013.

Zhu, Y., Rosenfeld, D., Yu, X., Liu, G., Dai, J., and Xu, X.: Satellite retrieval of convective cloud base temperature based on the NPP/VIIRS Imager, GEOPHYSICAL RESEARCH LETTERS, 41, 1308–1313, doi:10.1002/2013GL058970, 2014.

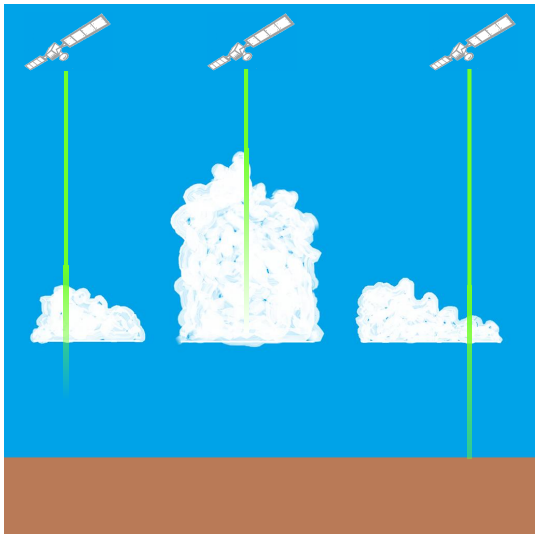

Figure 2. Schematic of CALIOP cloud base determination and evaluation strategy. In optically thick clouds (left and center), the lidar attenuates significantly within the cloud, rendering the cloud base information unreliable. However, the CBH of thin clouds (right) can be used as a proxy for thick clouds in a cloud field with homogeneous CBH.

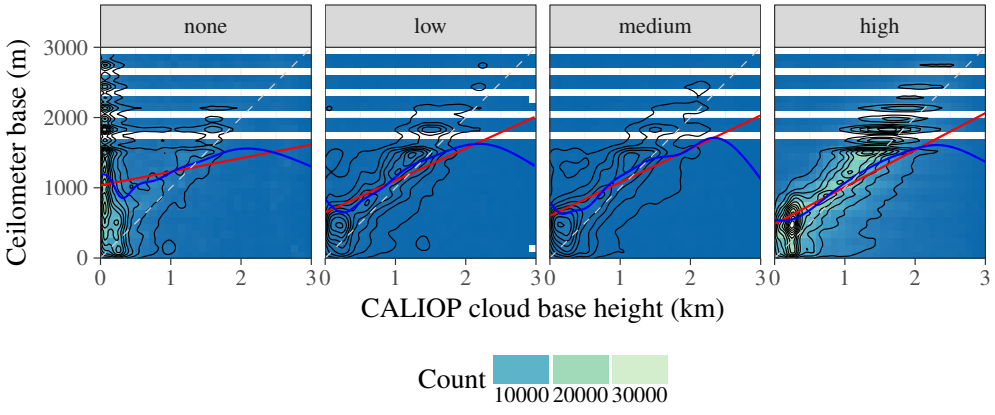

Figure 3. Scatter plots of CALIOP versus ceilometer local cloud base height faceted by the CALIOP VFM QA flag. Color indicates the number of CALIOP profiles within each bin of ceilometer and CALIOP CBH; black lines are contours of the empirical joint probability density; the red line is a linear least-squares fit, with 95% confidence interval shaded in light red; the blue line is a generalized additive model regression (Wood, 2011), with 95% confidence interval shaded in light blue; the dashed gray line is the one-to-one line. Statistics of the relationship between CALIOP and ceilometer base heights are provided in Table 1.

Table 1. Statistics of the relationship between ceilometer and CALIOP cloud base height faceted by CALIOP VFM QA flag. Shown are the number of CALIOP profiles n, the product-moment correlation coefficient r between CALIOP and ceilometer CBH, the RMSE, bias, and linear least-squares fit parameters.

feature.qa.lowest.cloud	n	r	RMSE (m)	bias (m)	fit
none	1410553	0.192	1.05×10^3	$-471.$	$y = 0.193x + 1.03 \times 10^3$ m
low	301250	0.471	710.	$-115.$	$y = 0.456x + 650.$ m
medium	212723	0.502	707.	-77.1	$y = 0.476x + 602.$ m
high	2877967	0.554	629.	9.85	$y = 0.526x + 485.$ m

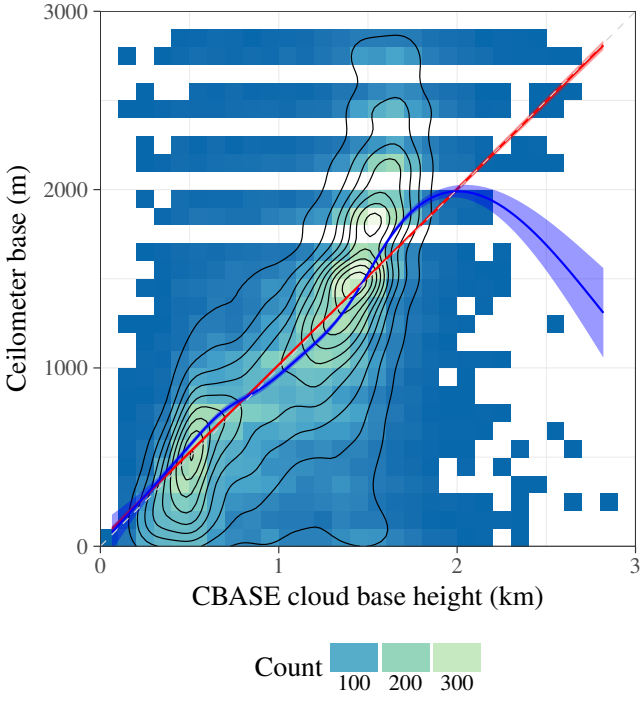

Figure 4. Scatter plot of CBASE versus ceilometer CBH for all A-Train overpasses over the CONUS available for 2007; for description of the plot elements, see Figure 3. The linear fit has slope 0.98 and intercept 33.96 m.

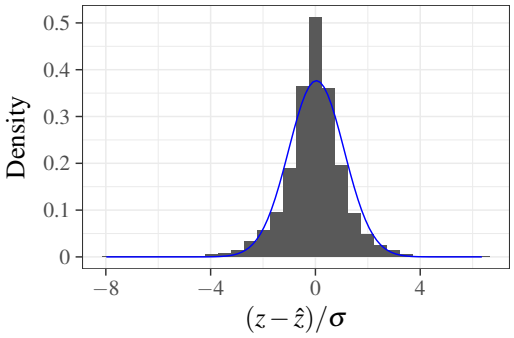

Figure 5. Distribution function of cloud base error divided by predicted uncertainty; for the ideal case of unbiased CBH and unbiased uncertainty, the distribution would be Gaussian with zero mean and unit standard deviation. The superimposed least-squares Gaussian fit (blue line) has mean 0.04 and standard deviation 1.06.

Table 2. CBASE cloud base statistics by decile of predicted uncertainty; see Table 1 for a description of the statistics provided.

pred.rmse	n	r	RMSE (m)	bias (m)	fit
(167,427]	2624	0.741	404.	−46.9	$y = 1.03x + 28.0$ m
(427,453]	2624	0.719	429.	−28.4	$y = 1.06x - 32.0$ m
(453,469]	2624	0.703	461.	−18.8	$y = 1.09x - 87.7$ m
(469,484]	2624	0.685	463.	−17.8	$y = 1.03x - 18.3$ m
(484,497]	2624	0.628	506.	−6.06	$y = 0.976x + 33.4$ m
(497,508]	2624	0.574	547.	−8.73	$y = 0.986x + 25.5$ m
(508,522]	2624	0.596	547.	−14.1	$y = 1.01x + 5.37$ m
(522,541]	2624	0.572	562.	−9.26	$y = 0.967x + 49.6$ m
(541,573]	2624	0.502	639.	−22.7	$y = 0.939x + 96.8$ m
(573,748]	2624	0.447	720.	7.36	$y = 0.829x + 197.$ m

Table 3. Statistics of the relationship between ceilometer and 2B-GEOPROF-LIDAR CBH; see Table 1 for a description of the statistics provided.

flag.base	n	r	RMSE (m)	bias (m)	fit
Radar	15061	0.265	782.	98.1	$y = 0.461x + 466.$ m
Lidar	12813	0.564	594.	16.3	$y = 0.555x + 399.$ m

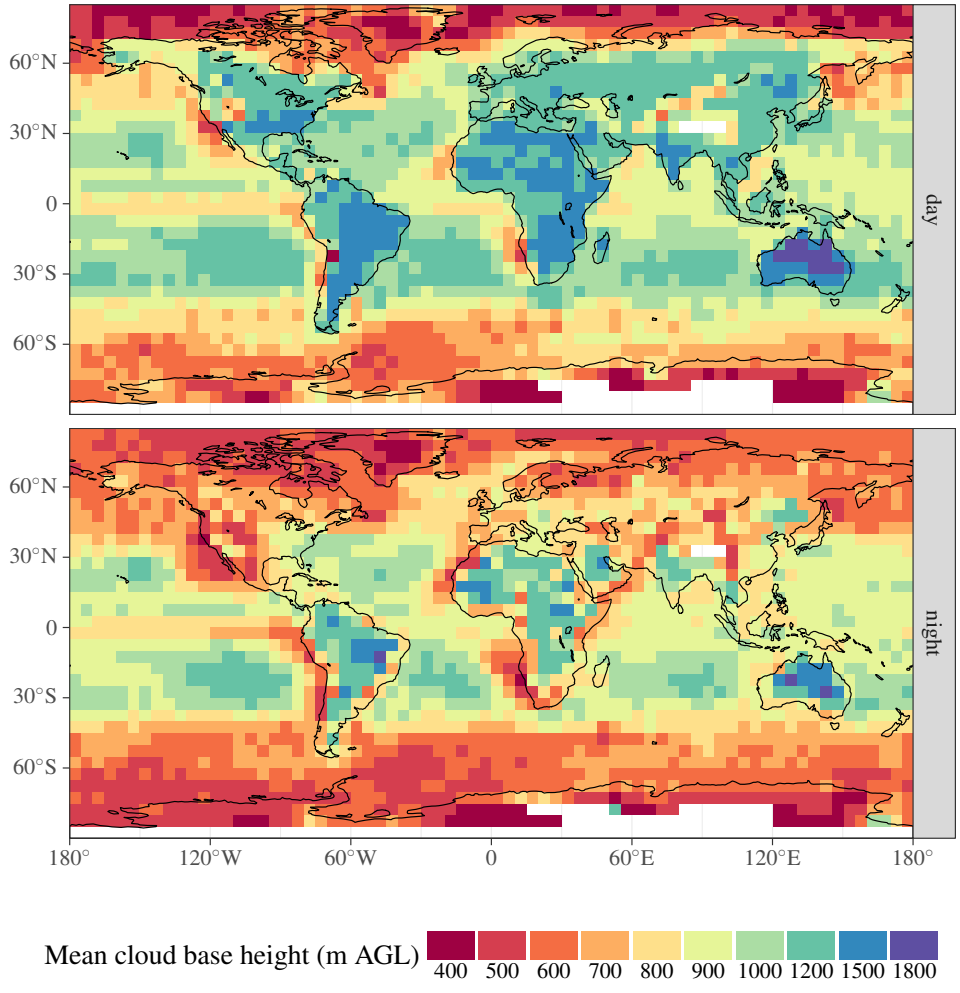

Figure 6. Geographic distribution of mean CBH above ground level. Statistics are calculated within each $5° \times 5°$ latitude–longitude box, and separately for CALIOP daytime (top) and nighttime (bottom) overpasses.

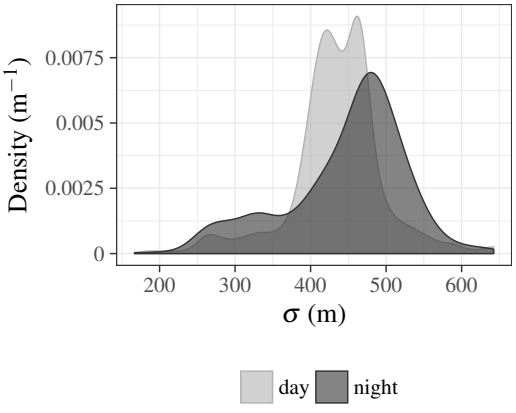

Figure 7. Distribution of predicted CBH uncertainty.

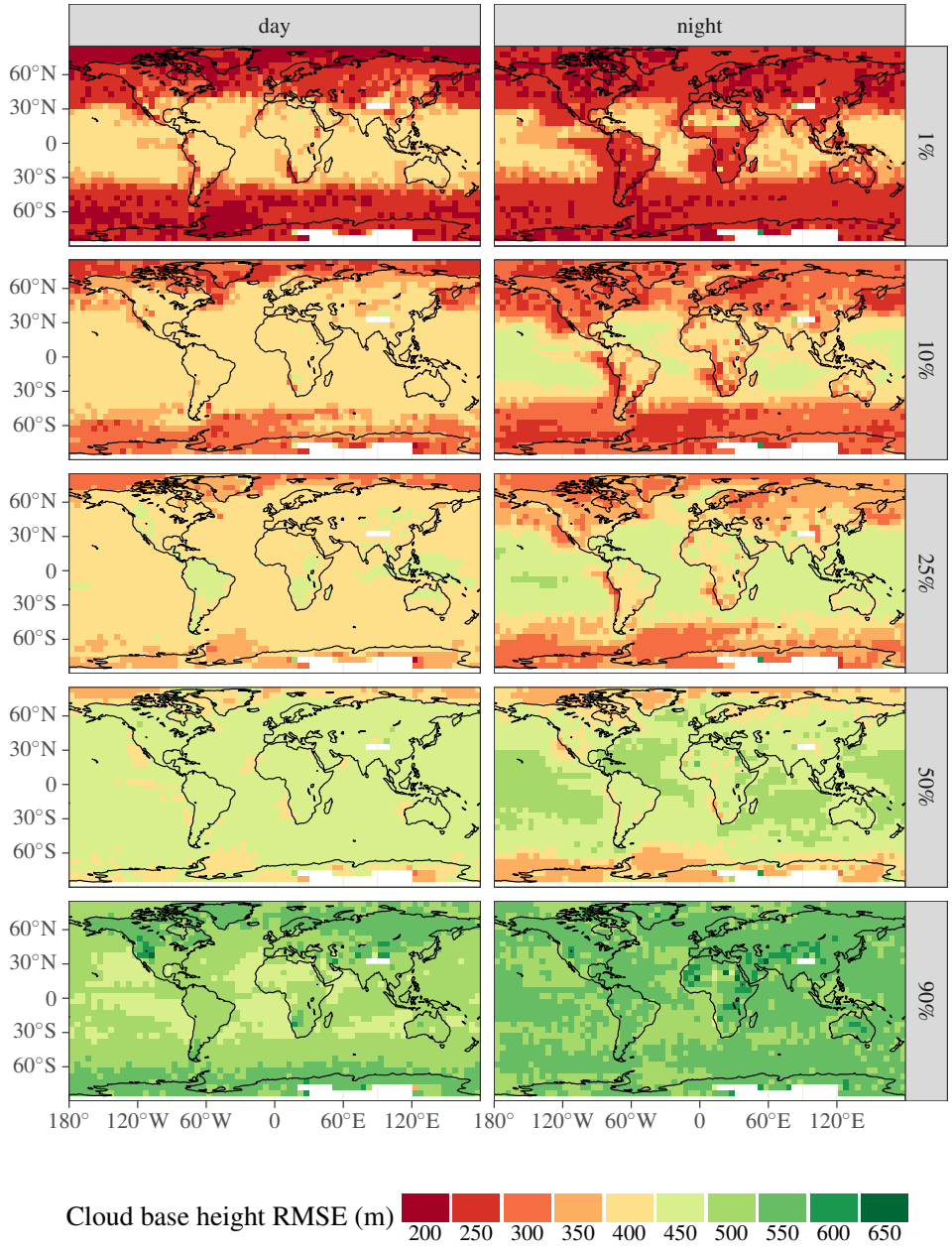

Figure 8. Cloud base uncertainty quantiles. Statistics are calculated within each 5° × 5° latitude–longitude box. The left (right) column shows statistics of daytime (nighttime) retrievals; daytime and nighttime are defined by the CALIOP VFM product.

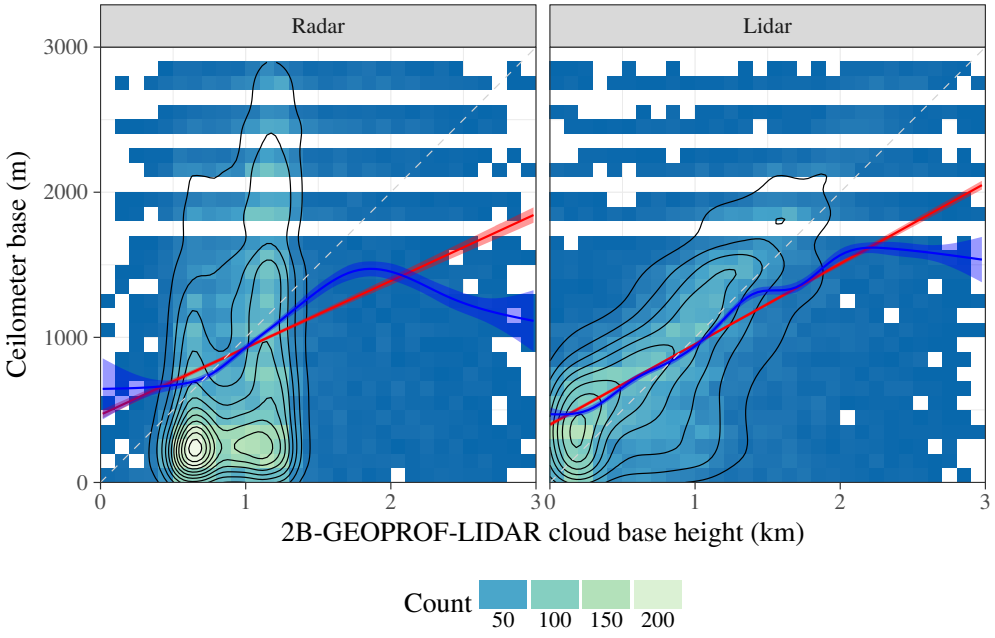

flag.base	n	r	RMSE (m)	bias (m)	fit
Radar	15061	0.265	782.	98.1	$y = 0.461x + 466.$ m
Lidar	12813	0.564	594.	16.3	$y = 0.555x + 399.$ m

Figure 9. Scatter plot of 2B-GEOPROF-LIDAR versus ceilometer CBH faceted by the source of the cloud base (radar-only or lidar-only; due to their rare occurrence, combined radar–lidar base heights are not shown). For description of the plot elements, see Figure 3. Statistics of the relationship between 2B-GEOPROF-LIDAR and ceilometer base heights are provided in Table 3.